Immuno-PET/CT Imaging of Trop2 with [^{18}F]AlF-RESCA-T4 Differentiates Lung Cancer from Inflammation

Wei Huang*[1], Min Cao*[2], Yanfei Wu*[3], You Zhang[1], Shuxian An[1], Xinbing Pan[1], Xinyuan Zhou[1], Hongda Shao[1], Yihui Guan[3], Gang Huang[1], Fabrizia Gelardi[4,5], Arturo Chiti[4,5], Fang Xie[3], Jianjun Liu[1], and Weijun Wei[1]

[1]*Department of Nuclear Medicine, Institute of Clinical Nuclear Medicine, School of Medicine, Renji Hospital, Shanghai Jiao Tong University, Shanghai, China;* [2]*Department of Thoracic Surgery, Renji Hospital, Shanghai Jiao Tong University School of Medicine, Shanghai, China;* [3]*Department of Nuclear Medicine and PET Center, Huashan Hospital, Fudan University, Shanghai, China;* [4]*Università Vita-Salute San Raffaele, Milan, Italy; and* [5]*Nuclear Medicine Department, IRCCS San Raffaele, Milano, Italy*

Immuno-PET/CT imaging, a branch of molecular imaging, can noninvasively and specifically visualize biomarker expression across the body. Trophoblast cell surface antigen 2 (Trop2) is a pan-cancer biomarker and plays a crucial role in tumorigenesis through multiple signaling pathways. The study aims to develop and translate novel Trop2 single-domain antibody (sdAb) tracers for clinical use. **Methods:** Two sdAbs (i.e., His-tagged T4 and His-tag−free RT4) are recombinantly expressed in Chinese hamster ovary cells. The purities and binding kinetics are determined by sodium dodecyl sulfate polyacrylamide gel electrophoresis, high-performance liquid chromatography, and surface plasmon resonance assays. The AlF restrained complexing agent (RESCA) method is applied to develop ^{18}F-labeled sdAb tracers ([^{18}F]AlF-RESCA-T4 and [^{18}F]AlF-RESCA-RT4), followed by thorough preclinical imaging and blocking studies on tumor-bearing mice and a pilot clinical trial evaluating the clinical imaging safety and feasibility of [^{18}F]AlF-RESCA-T4 immuno-PET/CT. **Results:** [^{18}F]AlF-RESCA-T4 and [^{18}F]AlF-RESCA-RT4 possess high radiochemical purities. Preclinical imaging in the T3M-4 tumor model revealed prominent uptake (percentage injected dose/g) of [^{18}F]AlF-RESCA-T4 (11.13 ± 1.53, $n = 4$) and [^{18}F]AlF-RESCA-RT4 (8.83 ± 1.22, $n = 4$), which were significantly reduced by coinjection of unlabeled T4 and RT4 in blocking studies. The His-tag removal strategy further optimized the probe's in vivo pharmacokinetics and reduced renal radioactivity accumulation without significantly decreasing tumor uptake. In a pilot clinical trial, [^{18}F]AlF-RESCA-T4 immuno-PET/CT showed promising potency in annotating Trop2 expression and differentiating tumors from inflammatory diseases such as tuberculosis. **Conclusion:** [^{18}F]AlF-RESCA-T4 and [^{18}F]AlF-RESCA-RT4 can specifically annotate Trop2 expression. Clinical [^{18}F]AlF-RESCA-T4 immuno-PET/CT imaging can screen patients for Trop2-targeted therapies and differentiate lung inflammation from cancer.

Key Words: Trop2; immuno-PET; single-domain antibody; companion diagnostics

J Nucl Med 2024; 65:1904–1910
DOI: 10.2967/jnumed.124.268751

Trophoblast cell surface antigen 2 (Trop2) is a glycoprotein that plays various roles in cell self-renewal, proliferation, transformation, and organ development. Encoded by the *TACSTD2* gene, Trop2 comprises a large extracellular domain, a single transmembrane domain, and a short intracellular tail. Trop2's pathophysiologic roles have become significant in the context of cancers, including triple-negative breast cancer (*1*), colorectal cancer (*2*), gastric carcinoma (*3*), pancreatic cancer (*4*), and non–small cell lung cancer (*5*), among others. Prooncogenic transcription factors and the inactivation of several transcription factors regulate its overexpression. Knocking out the *TACSTD2* gene disrupts tumor cell proliferation, further confirming the role of Trop2 in tumorigenesis.

Patient selection and response assessment are crucial aspects of molecularly targeted therapies. These processes help identify the most suitable patients for treatment and promptly evaluate their response to therapy. Biomarker testing is essential for guiding treatment decisions and response evaluations. Although immunohistochemistry is routinely used to determine the expression level of specific biomarkers, it has inherent disadvantages due to sampling biases, nonspecific background staining, and subjectivity in interpretation (*6,7*). Immunohistochemistry is primarily a qualitative technique and has limitations in accurately quantifying the antigen expression level. Tumors can exhibit spatial heterogeneity, in which different tumor regions may have distinct biomarker expression patterns (*8,9*). This can complicate the assessment of biomarker expression by immunohistochemistry, as a single biopsy sample may not fully represent the entire tumor and metastatic tumors across the body. Moreover, tumor heterogeneity can evolve because of clonal selection and the emergence of subclones with different genetic alterations. This dynamic heterogeneity can impact biomarker expression and treatment response, requiring periodic reassessment before and after the treatments.

Immuno-PET involves using radiolabeled antibodies or antibody fragments that specifically bind to the biomarkers of interest. This allows noninvasive imaging and quantification of biomarker expression in various tissues and organs across the body (*10*). Immuno-PET/CT imaging provides valuable insights into tumor biology, biomarker expression, patient selection, response assessment, and personalized treatment approaches by quantifying biomarker expression. As for Trop2, one study developed ^{89}Zr-labeled anti-Trop2 antibody (AF650) for immuno-PET/CT imaging in pancreatic cancer (*11*). Disadvantages of ^{89}Zr-labeled antibodies include a relatively high radiation dose to patients due to the long half-life of ^{89}Zr (78.4 h), repeated imaging within a week, limited availability of ^{89}Zr,

Received Sep. 5, 2024; revision accepted Oct. 22, 2024.
For correspondence or reprints, contact Weijun Wei (wwei@shsmu.edu.cn) or Jianjun Liu (ljjsh@sjtu.edu.cn).
*Contributed equally to this work.
Published online Nov. 14, 2024.

and dissociation of the ^{89}Zr from the antibody over time, affecting the reliability of the imaging results (*12*). Single-domain antibodies (sdAbs) are the smallest functional antibody fragments derived from camelid heavy-chain–only antibodies (*13,14*). The merits of high specificity and affinity, rapid targeting within 1 h, easy production and modification, and reduced immunogenicity make sdAbs excellent candidates for high-quality same-day immuno-PET imaging (*15,16*).

In efforts to develop same-day immuno-PET imaging tracers targeting Trop2, we first developed 2 sdAb tracers (i.e., [^{68}Ga]Ga-NOTA-RTD01 and [^{68}Ga]Ga-NOTA-RTD98), which revealed differential Trop2 expression in pancreatic cancer models but had high liver accumulation (*17*). We then screened 2 novel sdAbs with improved association and dissociation kinetics. Further, we developed ^{68}Ga-labeled sdAb tracers (i.e., [^{68}Ga]Ga-NOTA-T4 and [^{68}Ga]Ga-NOTA-T5), with [^{68}Ga]Ga-NOTA-T4 showing potential in patient stratification and differential diagnosis by visualizing heterogeneous Trop2 expression (*18*). The current work aimed to develop 2 ^{18}F-labeled sdAb tracers ([^{18}F]AlF-RESCA-T4 and [^{18}F]AlF-RESCA-RT4) and elucidate the impact of the His-tag on the tracers' pharmacokinetics and pharmacodynamics. After thorough preclinical evaluation, we further evaluated the imaging feasibility and differential diagnostic value of [^{18}F]AlF-RESCA-T4 immuno-PET in a pilot clinical trial.

MATERIALS AND METHODS

All materials and methods can be found in the supplemental materials online (available at http://jnm.snmjournals.org).

RESULTS

Characterization and Quality Control of T4

T4 has a molecular weight of about 15 kDa as detected by sodium dodecyl sulfate polyacrylamide gel electrophoresis (Fig. 1A). The purity of T4 was high, at more than 95% on high-performance liquid chromatography analysis (Fig. 1B). With a dissociation constant of 965.9 pM, T4 had a tight binding affinity with immobilized human Trop2 antigen as required for in vivo imaging. More importantly, no dissociation occurred after binding to the target protein (Fig. 1C). The chelator (±)-H_3RESCA-TFP conjugation did not significantly decrease the binding affinity to human Trop2 (Supplemental Fig. 1). The radiochemistry yield of [^{18}F]AlF-RESCA-T4 was approximately 22.4%. The radiochemical purity after purification was more than 99% (Fig. 1D), and [^{18}F]AlF-RESCA-T4 was stable within 2 h in phosphate-buffered saline and fetal bovine serum (Supplemental Fig. 2). The interaction fit curve of T4 and Trop2 demonstrated a fast association and a slow dissociation, indicating the rapid and tight binding necessary for subsequent imaging experiments.

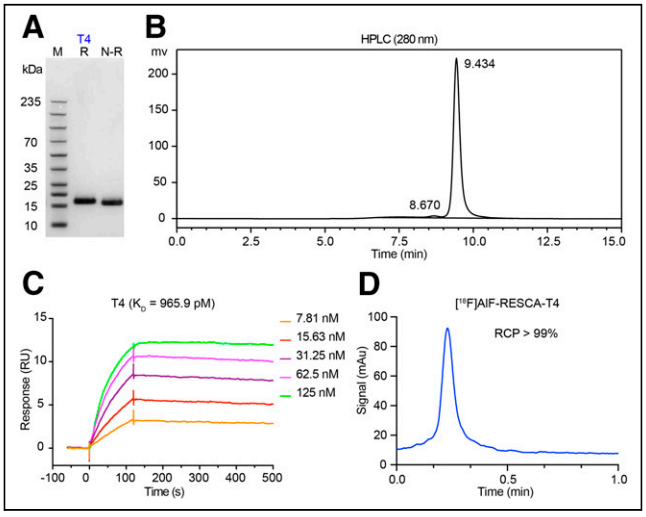

FIGURE 1. Characterization of T4 and quality control of [^{18}F]AlF-RESCA-T4. (A) Sodium dodecyl sulfate polyacrylamide gel electrophoresis of T4. (B) High-performance liquid chromatography–tested purity of T4. (C) Binding affinity between T4 and recombinant human Trop2 protein, as determined by SPR test. (D) Radiochemistry purity of [^{18}F]AlF-RESCA-T4 after purification. HPLC = high-performance liquid chromatography; K_D = dissociation constant; M = marker; N-R = nonreducing condition; R = reducing condition; RCP = radiochemistry purity; RU = response units.

[^{18}F]AlF-RESCA-T4 Immuno-PET/CT in Trop2-Positive CDX Model

In the Trop2-positive T3M-4 model, [^{18}F]AlF-RESCA-T4 immuno-PET/CT readily detected the tumor at 45 min after injection, as presented in Figure 2A. Region-of-interest (ROI) analysis showed an average tumor uptake of 11.13 ± 1.53 percentage injected dose (%ID)/g (n = 4, Fig. 2B). Besides, the kidney accumulation was high, with an average value of 125.60 ± 15.07 %ID/g (n = 4) due to urinary excretion, reabsorption, and retention. The uptake in other normal tissues and organs was generally low, indicating the excellent pharmacokinetics and stability of the tracer. Ex vivo biodistribution after the imaging similarly showed the highest accumulation in the kidneys followed by the uptake in the tumor, with corresponding values of 212.86 ± 20.60 %ID/g and 11.04 ± 1.88 %ID/g, respectively (n = 4, Fig. 2C). To validate the visualization specificity of [^{18}F]AlF-RESCA-T4, unlabeled T4 (400 μg) and [^{18}F]AlF-RESCA-T4 were coinjected in another group of tumor-bearing mice. Immuno-PET/CT imaging in the blocking group failed to visualize the Trop2-positive tumor (Fig. 2D). The quantitative ROI analysis (Fig. 2E) and biodistribution results (Fig. 2F) of the T4-blocking group demonstrated considerably low tumor uptake (2.33 ± 0.26 %ID/g and 2.45 ± 0.49 %ID/g, n = 4). T4 blocking also reduced accumulation in the liver and kidneys (Supplemental Fig. 3). Equivalently high membranous Trop2 expression was observed in the tumors of the 2 groups (Figs. 2G and 2H). These results demonstrated that [^{18}F]AlF-RESCA-T4 immuno-PET/CT can rapidly and precisely detect Trop2-positive tumors but with high kidney accumulation.

Expression and Characterization of His-Tag−Free RT4

To further investigate the impact of His-tag on the pharmacokinetics of sdAb tracer, we engineered His-tag−free RT4 from T4, which also had a molecular weight of approximately 15 kDa (Fig. 3A). As shown in Figure 3B, the purity of RT4 was over 95% on high-performance liquid chromatography analysis. The binding affinity of RT4 to recombinant human Trop2 protein was similar to that of T4, with a high dissociation constant of 915.7 pM (Fig. 3C). Similarly, chelator modification in preparing RESCA-RT4 did not significantly affect the interacting kinetics to recombinant human Trop2 protein (Supplemental Fig. 4). When compared with [^{18}F]AlF-RESCA-T4, [^{18}F]AlF-RESCA-RT4 had a higher radiochemistry yield (61.9% vs. 22.4%) and an equivalently high radiochemical purity (>99%, Fig. 3D).

[^{18}F]AlF-RESCA-RT4 Immuno-PET/CT in Trop2-Positive CDX Model

At 2 time points (45 min and 2.5 h), [^{18}F]AlF-RESCA-RT4 immuno-PET/CT imaging was also performed on the T3M-4

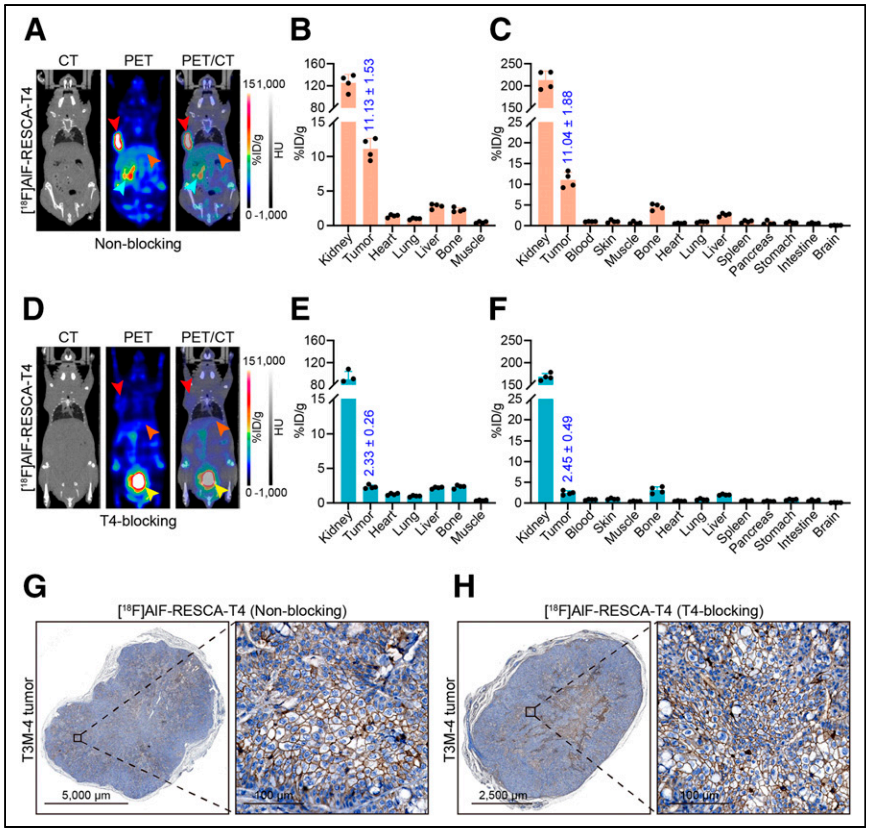

FIGURE 2. [^{18}F]AlF-RESCA-T4 immuno-PET/CT imaging of Trop2-positive T3M-4 model. (A and D) Representative [^{18}F]AlF-RESCA-T4 immuno-PET/CT images of nonblocking (A) and T4-blocking (D) groups. (B and E) ROI analysis of nonblocking (n = 4, B) and T4-blocking (n = 4, E) groups. Tumor uptake of [^{18}F]AlF-RESCA-T4 was significantly higher in nonblocking group than in T4-blocking group. (C and F) Ex vivo biodistribution data of 2 groups (n = 4/group). (G and H) Immunohistochemistry staining results of tumor tissues from 2 groups. Red arrowhead indicates tumor; orange arrowhead, liver; blue arrowhead, kidney; and yellow arrowhead, bladder. HU = Hounsfield units.

model to investigate the differential clearance patterns and diagnostic value. Representative static images are presented in Figure 4A. Tumor uptake of [^{18}F]AlF-RESCA-RT4 was stably high at the 2 time points (8.80 ± 2.21 %ID/g at 45 min and 8.83 ± 1.22 %ID/g at 2.5 h, n = 4; Fig. 4B), with a clean background. Uptake was lower in major organs and tissues, including the heart, lung, liver, bone, and muscle, except for the kidneys (Fig. 4B). Unlike the stable tumor uptake, uptake in the kidney, heart, lung, liver, and muscle decreased over time. The uptake in bone mildly increased from 45 min to 2.5 h after injection (1.11 ± 0.50 %ID/g and 1.28 ± 0.22 %ID/g, respectively). We also confirmed the targeting specificity of [^{18}F]AlF-RESCA-RT4 with excess RT4 as the coinjection blocking agent. A 400-μg quantity of RT4 was coinjected with [^{18}F]AlF-RESCA-RT4 into the tumor-bearing mice to saturate Trop2 molecules on tumor cells. After RT4 blocking, tumor uptake of [^{18}F]AlF-RESCA-RT4 was comparable to that in normal tissues and organs (Figs. 4C and 4D). Although retention and uptake in the heart, lung, and muscle decreased at delayed imaging, the tumor uptake did not show a significant decrease at 45 min (2.13 ± 0.67 %ID/g) or 2.5 h (2.08 ± 0.28 %ID/g) in the RT4-blocking group. Tumor uptake was significantly lower in the RT4-blocking group than in the nonblocking group (2.08 ± 0.28 %ID/g vs. 8.83 ± 1.22 %ID/g, P < 0.01; Supplemental Fig. 5A). Comparison of the biodistribution results in the 2 groups confirmed significantly declined tumor uptake in the RT4-blocking group (8.41 ± 2.69 %ID/g vs. 2.75 ± 0.67 %ID/g, P < 0.01; Supplemental Fig. 5B). High Trop2 expression was confirmed in tumor tissues of both experimental groups through immunohistochemistry staining (Supplemental Figs. 5C and 5D). Thus, [^{18}F]AlF-RESCA-RT4 immuno-PET/CT also rapidly and specifically detected Trop2-positive tumors with reduced kidney accumulation.

Head-to-Head Comparison of [^{18}F]AlF-RESCA-T4, [^{18}F]AlF-RESCA-RT4, and [^{68}Ga]Ga-NOTA-T4

We previously developed [^{68}Ga]Ga-NOTA-T4 for clinical use (*18*), and we further developed [^{18}F]AlF-RESCA-T4 and [^{18}F]AlF-RESCA-RT4 in the current work. Here, we compare the different pharmacokinetics and pharmacodynamics of the 3 tracers. The His-tagged [^{18}F]AlF-RESCA-T4 showed a high renal radioactivity accumulation of 125.60 ± 15.07 %ID/g (n = 4) on ROI analysis. A head-to-head comparison with [^{18}F]AlF-RESCA-T4 showed that the His-tag−free [^{18}F]AlF-RESCA-RT4 exhibited a significant decrease in kidney accumulation (48.88 ± 8.93 %ID/g vs. 125.60 ± 15.07 %ID/g, n = 4 per group, P < 0.01; Supplemental Fig. 6A), which was further validated by biodistribution analysis results (Supplemental Fig. 6B). Tumor uptake of [^{18}F]AlF-RESCA-RT4 was lower than that of [^{18}F]AlF-RESCA-T4 on ROI analysis (8.83 ± 1.22 %ID/g vs. 11.13 ± 1.53 %ID/g, n = 4) and also on biodistribution analysis (8.41 ± 2.69 %ID/g vs. 11.04 ± 1.88 %ID/g, n = 4). However, the decrease was not statistically meaningful (P > 0.05). [^{18}F]AlF-RESCA-RT4 had a clearer imaging background with significantly reduced uptake in the blood pool, muscle, bone, heart, lung, liver, spleen, stomach, and muscle (Supplemental Fig. 6B). These results demonstrated that the His-tag removal strategy improved [^{18}F]AlF-RESCA-RT4 immuno-PET/CT imaging performance, with reduced kidney accumulation and background uptake.

When comparing the performance of the 3 tracers together, we found that [^{18}F]AlF-RESCA-T4 and [^{18}F]AlF-RESCA-RT4 had higher tumor uptake than [^{68}Ga]Ga-NOTA-T4 (Supplemental Figs. 6C−6E). Although [^{68}Ga]Ga-NOTA-T4 had a better tumor-to-bone ratio, delayed immuno-PET/CT imaging at 2.5 h with [^{18}F]AlF-RESCA-RT4 showed a superior tumor-to-muscle ratio, tumor-to-liver ratio, and tumor-to-kidney ratio (Supplemental Fig. 6F). Maximum-intensity projection and transversal images in Supplemental Figures 7A–7D showed the kidney accumulation of [^{68}Ga]Ga-NOTA-T4 (45 min), [^{18}F]AlF-RESCA-T4 (45 min), and [^{18}F]AlF-RESCA-RT4 (45 min and 2.5 h). From the ROI (Supplemental Fig. 7E) and biodistribution (Supplemental Fig. 7F) analysis results, we can conclude that delayed immuno-PET/CT imaging with [^{18}F]AlF-RESCA-RT4 showed the best target-to-background ratio mainly

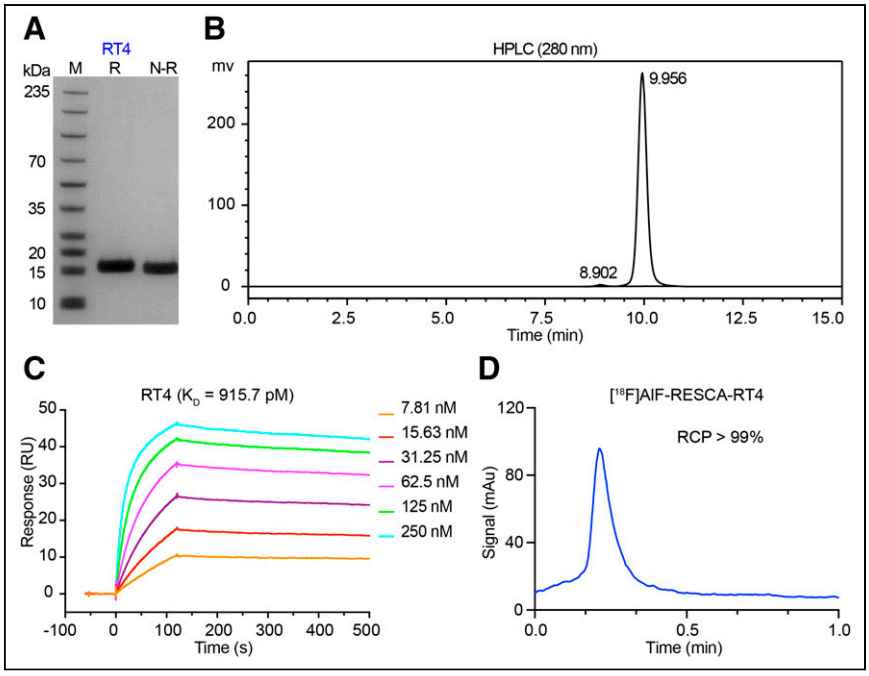

FIGURE 3. Characterization of RT4 and quality control of [^{18}F]AlF-RESCA-RT4. (A and B) Purity of RT4 as tested by sodium dodecyl sulfate polyacrylamide gel electrophoresis and high-performance liquid chromatography. (C) SPR test–determined binding affinity between RT4 and recombination human Trop2. (D) Radiochemistry purity of [^{18}F]AlF-RESCA-RT4 after purification. HPLC = high-performance liquid chromatography; K_D = dissociation constant; M = marker; N-R = nonreducing condition; R = reducing condition; RCP = radiochemistry purity; RU = response units.

because of the retained tumor uptake and significantly reduced kidney accumulation.

[^{18}F]AlF-RESCA-T4 Immuno-PET/CT in Suspected Lung Cancer Patients

In an ongoing clinical trial (ClinicalTrials.gov ID NCT06203574), we are exploring the clinical imaging safety and diagnostic value of [^{18}F]AlF-RESCA-T4. Here, we present 3 representative cases (2 women and 1 man) highlighting the value of [^{18}F]AlF-RESCA-T4 immuno-PET/CT imaging. No adverse events were observed within 4 h after injection of [^{18}F]AlF-RESCA-T4.

Patient 1 was a man with a left hilar nodule whose preoperative contrast-enhanced CT (CECT) scan revealed additional enlarged lymph nodes with enhancement in the mediastinum (paraaortic arch and subaortic arch) and left hilar regions (Supplemental Fig. 8), suggesting primary left hilar malignancy accompanied by left hilar and mediastinal lymph node metastases. [^{18}F]AlF-RESCA-T4 immuno-PET/CT imaging demonstrated prominent tracer uptake in the left hilar nodule (20.0 × 17.0 mm) and left hilar lymph node (19.9 × 19.3 mm), with a corresponding SUV_{max} of 10.69 and 10.12, respectively (Figs. 5A–5C). Notably, diffuse uptake of [^{18}F]AlF-RESCA-T4 (SUV_{max} of 7.42) was also observed in the left lower lung atelectasis caused by the primary tumor. This patient then received a mediastinoscopic biopsy of the suspected lymph nodes on CECT, and a pathologic examination revealed an inflammatory station 4 L lymph node (SUV_{max} of 0.9) with negative Trop2 expression despite the enhancement on CECT (Supplemental Figs. 9A and 9B). After exclusion of the potential mediastinal lymph node metastases, the patient underwent a sleeve resection of the left lower lobe of the lung. Pathologic examination of surgical specimens confirmed primary left hilar cancer with left hilar lymph node metastases. Immunohistochemistry staining confirmed intense Trop2 expression in the primary tumor (Fig. 5D) and metastatic left hilar lymph node (Supplemental Figs. 9C and 9D). The collapsed left lower lung tissue was also collected and stained for Trop2 expression. We observed moderate Trop2 expression in alveolar cells and intense Trop2 expression in club and ciliated bronchiole cells (Supplemental Figs. 9E and 9F). Still, overall expression in normal lung cells (alveolar cells, club cells, and ciliated cells) was lower than in tumor tissues, allowing precise identification of the primary tumor and metastatic lymph node in the patient. [^{18}F]AlF-RESCA-T4 immuno-PET/CT imaging of the patient changed the staging and clinical decision-making after multidisciplinary discussion.

Patient 2 was a woman with a left upper lung nodule, in which preoperative CECT showed gradual enhancement (Supplemental Fig. 10). The [^{18}F]AlF-RESCA-T4 immuno-PET/CT was harnessed to visualize Trop2 expression of the nodule and facilitate an auxiliary diagnosis. The nodule showed slight uptake, with an SUV_{max} of 1.55 (Figs. 6A–6C). Albeit low, the

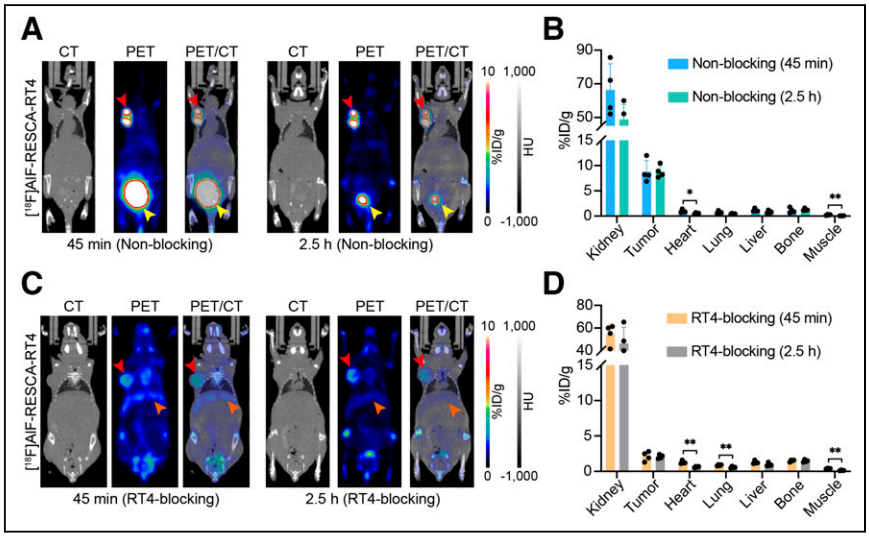

FIGURE 4. [^{18}F]AlF-RESCA-RT4 immuno-PET/CT imaging of Trop2-positive T3M-4 model. (A and C) At 2 time points (45 min and 2.5 h), images of nonblocking (A) and RT4-blocking (C) groups after [^{18}F]AlF-RESCA-RT4 injection. (B and D) ROI quantitative analysis of 2 groups (n = 4/group) at 45 min and 2.5 h after injection. Red arrowhead indicates tumor; orange arrowhead, liver; and yellow arrowhead, bladder. *P < 0.05. **P < 0.01.

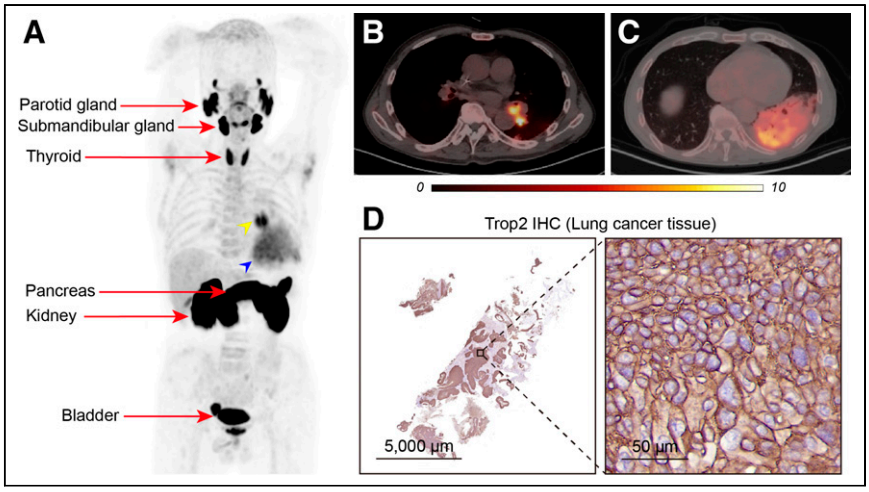

FIGURE 5. [^{18}F]AlF-RESCA-T4 immuno-PET/CT imaging of patient with primary lung cancer. (A–C) Maximum-intensity projection (A) and fusion images (B and C) of [^{18}F]AlF-RESCA-T4 immuno-PET/CT. Yellow arrowhead indicates presence of left hilar occupancy and lymph node in fusion image. Blue arrowhead indicates presence of distal lung atelectasis. Physiologic uptake of [^{18}F]AlF-RESCA-T4 by normal organs and tissues is indicated by red arrows. (D) Histologic examination of resected left hilar mass showed intense Trop2 staining. IHC = immunohistochemistry.

uptake was still higher than the background lung uptake (SUV_{max} of 0.26). Postoperative pathologic examination indicated the presence of lung adenocarcinoma and intense Trop2 staining on tumor cells (Figs. 6D and 6E). Similarly, positive alveolar, club, and ciliated cell expression can be found in staining results of normal lung tissue (Supplemental Fig. 11).

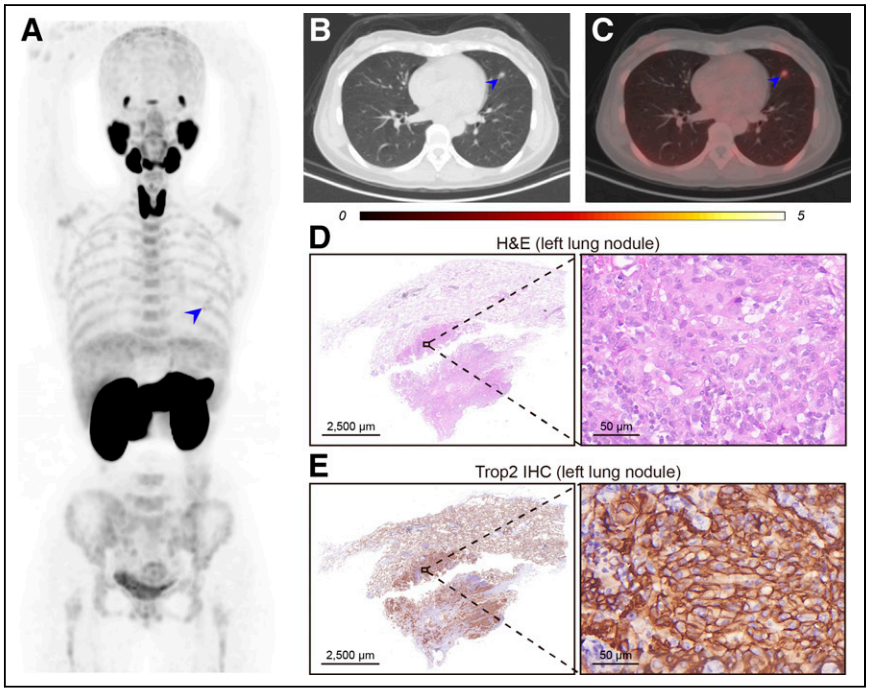

FIGURE 6. [^{18}F]AlF-RESCA-T4 immuno-PET/CT imaging of patient with lung adenocarcinoma. (A–C) Maximum-intensity projection image (A), CT (B), and fusion image (C) of [^{18}F]AlF-RESCA-T4 immuno-PET/CT. Blue arrowheads indicate location of left lung nodule. (D and E) Results of hematoxylin and eosin (D) and Trop2 immunohistochemistry (E) staining of surgically resected left lung nodule. H&E = hematoxylin and eosin; IHC = immunohistochemistry.

Patient 3 was a 49-y-old woman who presented for a comprehensive evaluation of an exemplary mass in the front of the right chest wall. With all the tumor biomarkers being negative, the patient first underwent ^{18}F-FDG PET/CT scanning, which showed the mass to be infiltrating the adjacent muscle, the right clavicle, and the right first rib. Moreover, there was a right apical pleura nodule, left hilar mass, liver mass, uterine nodule, and enlarged mediastinal and retroperitoneal lymph nodes with intense ^{18}F-FDG uptake (SUV_{max}, 25.2 − 42.0) (Supplemental Figs. 12A−12D). The imaging results indicated possible malignant tumors or lymphoma, but tuberculosis could not be excluded. The patient was recruited for [^{18}F]AlF-RESCA-T4 immuno-PET/CT imaging. All nodules were negative for [^{18}F]AlF-RESCA-T4 uptake (Supplemental Figs. 12E−12H), indicating that the diffuse findings were not typical lung adenocarcinoma or squamous carcinoma (our unpublished data [2024] show that most cases of lung adenocarcinoma and squamous carcinoma are Trop2-positive). Biopsy and histopathologic examination of the chest wall mass created a high suspicion of tuberculosis with negative Trop2 staining (Supplemental Figs. 12I and 12J). The next-generation sequencing of the biopsied tissue showed infiltration of the *Mycobacterium tuberculosis* complex. This was confirmed by positive T-SPOT.*TB* (Oxford Immunotec Ltd.) testing and tuberculosis antigens. A final diagnosis of tuberculosis was established, and antituberculosis treatment was then initiated. This case indicates the potential value of [^{18}F]AlF-RESCA-T4 immuno-PET/CT in differentiating inflammatory disease from typical lung cancers (i.e., adenocarcinoma and squamous carcinoma).

DISCUSSION

Previous studies have reported that monoclonal antibody–derived immuno-PET imaging tracers targeting Trop2 have achieved good diagnostic efficacy in preclinical models (*11,19*). However, clinical translation and use of these long-half-life radiometal-labeled tracers face practical difficulties because of the scarcity of long-half-life radiometals and weeklong imaging at multiple time points (*10*). In this setting, same-day immuno-PET imaging with tracers derived from low-molecular-weight vectors is favored for routine clinical application. SdAb is among the most potent targeting vectors because of its high binding affinity, excellent stability, and versatile engineering potential (*16*).^{68}Ga and ^{18}F are the 2 most applied radionuclides for labeling low-molecular-weight vectors. However,

traditional ^{18}F labeling methods involving harsh conditions generally do not apply to heat-sensitive biomolecules such as antibodies. The recent introduction of bioorthogonal chemistry in radiopharmaceuticals provided new solutions for developing ^{18}F-labeled sdAb tracers (*20,21*). Still, time-consuming 2-step or multiple-step labeling procedures are generally required for bioorthogonal chemistry-mediated labeling to avoid the impact of high temperatures on the structure and function of biomolecules (*22,23*). The chelator TFP-H_3RESCA, also known as (±)-H_3RESCA-TFP, is a tetrafluorophenyl ester derivative of RESCA. It has been increasingly used for ^{18}F labeling of biomolecules through amine coupling, explicitly targeting the N terminus or the ε-amino groups of lysine residues (*24*). The bifunctional chelator is well compatible with heat-sensitive biomolecules. It is further characterized by 1-step mild labeling at room temperature (~20°C) in an aqueous medium and, more importantly, high radiochemical yield and purity. Previous studies have confirmed the favorable pharmacokinetics and high in vivo stability of sdAb tracers developed by [^{18}F]AlF-RESCA labeling (*25–27*).

Our work developed the sdAb-derived tracer ([^{18}F]AlF-RESCA-T4) targeting Trop2 with high radiochemical yield and excellent radiochemical purity. High and specific tumor uptake of [^{18}F]AlF-RESCA-T4 in the pancreatic cancer T3M-4 model was observed. However, predominant kidney accumulation of the tracer was also observed. Blocking with excess cold T4 statistically reduced kidney accumulation of the tracer (89.85 ± 14.23 %ID/g vs. 125.60 ± 15.07 %ID/g, $n = 4$) in addition to reducing tumor uptake (2.33 ± 0.26 %ID/g vs. 11.13 ± 1.53 %ID/g, $n = 4$). Because of its overexpression in cancer cells and its involvement in tumorigenesis, Trop2 has gained attention as a potential therapeutic target, offering a promising avenue for developing more effective cancer treatments. Targeting Trop2 presents a promising and selective approach to cancer treatment, with the potential to minimize damage to normal cells. Since sacituzumab govitecan's clinical approval, more than 50 clinical trials have evaluated Trop2-targeted therapeutics (*28–30*). This significant interest in Trop2 as a therapeutic target underscores its potential to revolutionize cancer treatment. The kidney accumulation was still too high and may lead to nephrotoxicity when switching diagnostic radionuclides to therapeutic or theranostic radionuclides such as ^{177}Lu and ^{225}Ac. Indeed, in pursuing radiotheranostics in oncology (*31,32*), toxicity associated with therapeutic radiopharmaceuticals is a core problem to be addressed. Coadministration of small molecules such as maleate and fructose may decrease kidney accumulation of radiometal-labeled sdAb tracers (*33*). Still, this approach may not apply to human subjects because of the inherent toxicity of these small molecules. In the current work, we removed the His-tag on the sdAb T4 and developed the His-tag−free sdAb tracer [^{18}F]AlF-RESCA-RT4. We found that this simple engineering step substantially reduced kidney accumulation (48.88 ± 8.93 %ID/g vs. 125.60 ± 15.07 %ID/g, $n = 4$) without significantly compromising tumor uptake (8.83 ± 1.22 %ID/g vs. 11.13 ± 1.53 %ID/g, $n = 4$). Our ongoing work is exploiting other strategies to synergistically reduce kidney retention of radiometal-labeled sdAb radiopharmaceuticals to create windows for integrated immuno-PET/CT imaging and radioimmunotherapy (*34*). In our preclinical studies, delayed immuno-PET/CT imaging with [^{18}F]AlF-RESCA-RT4 showed significantly lower kidney, liver, and bone accumulation than [^{18}F]AlF-RESCA-T4 (Supplemental Fig. 6). Bone and liver accumulation of [^{18}F]AlF-RESCA-T4 might compromise the detection of metastases at these sites. Therefore, clinical translation of [^{18}F]AlF-RESCA-RT4 may improve imaging contrast and diagnostic value. Translation of [^{18}F]AlF-RESCA-RT4 on the uEXPLORER (United Imaging) total-body PET/CT scanner, which enables dynamic imaging, will be performed in late 2024.

With increasing numbers of Trop2-specific antibody therapeutics entering clinical trials, there is an unmet clinical demand to noninvasively visualize the heterogeneous and dynamic expression of Trop2 across the treatment cycle. Since we are still optimizing the purification methods for the His-tag−free RT4 to meet clinical translational requirements, we first translated [^{18}F]AlF-RESCA-T4 for clinical use, as purification of the His-tagged T4 is straightforward (*18*). [^{18}F]AlF-RESCA-T4 immuno-PET/CT imaging showed good imaging safety and distribution profiles in the initial 3 patients. Preoperative CECT of patient 1 revealed the left hilar mass associated with distal atelectasis and the presence of enlarged and enhanced left hilar and mediastinal lymph nodes highly suggestive of metastases. Since [^{18}F]AlF-RESCA-T4 immuno-PET/CT was negative for tracer uptake in the suggestive mediastinal lymph nodes, a mediastinoscopic biopsy was applied, and pathologic examination demonstrated that the mediastinal lymph nodes were inflammatory rather than metastatic. Consequently, a sleeve resection approach was selected for the patient. The [^{18}F]AlF-RESCA-T4 immuno-PET/CT imaging results correlated well with the postoperative pathology and immunohistochemistry staining results. In patient 2, with an early-stage adenocarcinoma in the left upper lung, [^{18}F]AlF-RESCA-T4 uptake also correlated well with the positive Trop2 expression. However, in patient 3, with tuberculosis involving multiple organs and tissues, ^{18}F-FDG uptake but not [^{18}F]AlF-RESCA-T4 uptake was observed. Our unpublished data (2024) show that Trop2 is highly expressed in lung adenocarcinoma and lung squamous carcinoma, but its expression in tuberculosis, sarcoidosis, and other inflammatory diseases is generally low. Differential Trop2 expression patterns indicate the differential diagnostic potential of Trop2-targeted imaging in diagnostic dilemmas (*18*). Further clinical trials on large patient cohorts are required to support our preliminary conclusion.

Trop2 is expressed at varying levels in normal tissues, including the epithelial secretory tissue of the endocrine and exocrine glands, kidneys (distal convoluted tubules and collecting ducts), lung (alveolar cells, club cells, and ciliated cells), and pancreas (pancreatic duct cells and acinar cells), and this positive expression can also be detected from the results of single-cell sequencing in public databases (https://www.proteinatlas.org/) (*35,36*). Despite the broad-range expression of Trop2 in normal tissues, albeit at different levels, our immuno-PET/CT imaging results disclosed predominant uptake of the tracer bilaterally in the salivary glands, as well as in the thyroid, pancreas, and prostate, which may turn out to be organs vulnerable to on-target, off-tumor toxicities when Trop2-targeted therapeutics are administered. In addition to selecting patients and facilitating differential diagnoses, the added value of [^{18}F]AlF-RESCA-T4 immuno-PET/CT in predicting or monitoring treatment-related adverse effects also needs to be investigated.

CONCLUSION

We successfully developed 2 ^{18}F-labeled sdAb tracers, [^{18}F]AlF-RESCA-T4 and [^{18}F]AlF-RESCA-RT4, with the latter showing substantially reduced kidney accumulation. Initial clinical [^{18}F]AlF-RESCA-T4 immuno-PET/CT imaging demonstrated the

ability to visualize Trop2 expression and the associated differential diagnostic value in lung diseases.

DISCLOSURE

This work was supported in part by the National Key Research and Development Program of China (grant 2020YFA0909000), the National Natural Science Foundation of China (grant 82372014), and the Shen Kang-United Imaging Joint Research and Development Plan (grant SKLY2022CRT301). Weijun Wei, Wei Huang, and Jianjun Liu are coinventors on a provisional patent application encompassing the technology reported in the manuscript. Weijun Wei is a consultant of Alpha Nuclide (Ningbo) Medical Technology Co., Ltd. No other potential conflict of interest relevant to this article was reported.

KEY POINTS

QUESTION: Trop2, a pan-cancer biomarker, has great theranostic potential in solid tumors. Can we noninvasively annotate Trop2 expression in solid tumors and inflammation?

PERTINENT FINDINGS: We developed novel sdAb tracers targeting Trop2 and translated [^{18}F]AlF-RESCA-RT4 for clinical use. Immuno-PET/CT imaging with [^{18}F]AlF-RESCA-RT4 precisely visualized Trop2 expression in preclinical models and patients, allowing the selection of patients for Trop2-targeted treatments and differentiation of cancers from inflammatory diseases.

IMPLICATIONS FOR PATIENT CARE: Clinical incorporation of the imaging approach may substantially improve Trop2-targeted cancer theranostics by noninvasive target visualization, patient stratification, response monitoring, and differential diagnoses.

REFERENCES

1. Bardia A, Hurvitz SA, Tolaney SM, et al. Sacituzumab govitecan in metastatic triple-negative breast cancer. *N Engl J Med.* 2021;384:1529–1541.
2. Ohmachi T, Tanaka F, Mimori K, Inoue H, Yanaga K, Mori M. Clinical significance of TROP2 expression in colorectal cancer. *Clin Cancer Res.* 2006;12:3057–3063.
3. Mühlmann G, Spizzo G, Gostner J, et al. TROP2 expression as prognostic marker for gastric carcinoma. *J Clin Pathol.* 2009;62:152–158.
4. Fong D, Moser P, Krammel C, et al. High expression of TROP2 correlates with poor prognosis in pancreatic cancer. *Br J Cancer.* 2008;99:1290–1295.
5. Parisi C, Mahjoubi L, Gazzah A, Barlesi F. TROP-2 directed antibody-drug conjugates (ADCs): the revolution of smart drug delivery in advanced non-small cell lung cancer (NSCLC). *Cancer Treat Rev.* 2023;118:102572.
6. Chen PL, Roh W, Reuben A, et al. Analysis of immune signatures in longitudinal tumor samples yields insight into biomarkers of response and mechanisms of resistance to immune checkpoint blockade. *Cancer Discov.* 2016;6:827–837.
7. Hegde PS, Karanikas V, Evers S. The where, the when, and the how of immune monitoring for cancer immunotherapies in the era of checkpoint inhibition. *Clin Cancer Res.* 2016;22:1865–1874.
8. Burrell RA, McGranahan N, Bartek J, Swanton C. The causes and consequences of genetic heterogeneity in cancer evolution. *Nature.* 2013;501:338–345.
9. Moek KL, Giesen D, Kok IC, et al. Theranostics using antibodies and antibody-related therapeutics. *J Nucl Med.* 2017;58(suppl 2):83S–90S.
10. Wei W, Rosenkrans ZT, Liu J, Huang G, Luo QY, Cai W. ImmunoPET: concept, design, and applications. *Chem Rev.* 2020;120:3787–3851.
11. Chen W, Li M, Younis MH, et al. ImmunoPET of trophoblast cell-surface antigen 2 (Trop-2) expression in pancreatic cancer. *Eur J Nucl Med Mol Imaging.* 2022;49:861–870.
12. Chames P, Van Regenmortel M, Weiss E, Baty D. Therapeutic antibodies: successes, limitations and hopes for the future. *Br J Pharmacol.* 2009;157:220–233.
13. Ingram JR, Schmidt FI, Ploegh HL. Exploiting nanobodies' singular traits. *Annu Rev Immunol.* 2018;36:695–715.
14. Jumapili NA, Zivalj M, Barthelmess RM, et al. A few good reasons to use nanobodies for cancer treatment. *Eur J Immunol.* 2023;53:e2250024.
15. Krasniqi A, D'Huyvetter M, Devoogdt N, et al. Same-day imaging using small proteins: clinical experience and translational prospects in oncology. *J Nucl Med.* 2018;59:885–891.
16. Wei W, Younis MH, Lan X, Liu J, Cai W. Single-domain antibody theranostics on the horizon. *J Nucl Med.* 2022;63:1475–1479.
17. Huang W, Liang C, Zhang Y, et al. ImmunoPET imaging of Trop2 expression in solid tumors with nanobody tracers. *Eur J Nucl Med Mol Imaging.* 2024;51:380–394.
18. Huang W, Zhang Y, Cao M, et al. ImmunoPET imaging of Trop2 in patients with solid tumours. *EMBO Mol Med.* 2024;16:1143–1161.
19. Sperger JM, Helzer KT, Stahlfeld CN, et al. Expression and therapeutic targeting of TROP-2 in treatment-resistant prostate cancer. *Clin Cancer Res.* 2023;29:2324–2335.
20. Meyer JP, Adumeau P, Lewis JS, Zeglis BM. Click chemistry and radiochemistry: the first 10 years. *Bioconjug Chem.* 2016;27:2791–2807.
21. Bauer D, Cornejo MA, Hoang TT, Lewis JS, Zeglis BM. Click chemistry and radiochemistry: an update. *Bioconjug Chem.* 2023;34:1925–1950.
22. Wei W, Zhang D, Wang C, et al. Annotating CD38 expression in multiple myeloma with [^{18}F]F-Nb1053. *Mol Pharm.* 2022;19:3502–3510.
23. Zhou Z, Zalutsky MR, Vaidyanathan G. Labeling a TCO-functionalized single domain antibody fragment with ^{18}F via inverse electron demand Diels Alder cycloaddition using a fluoronicotinyl moiety-bearing tetrazine derivative. *Bioorg Med Chem.* 2020;28:115634.
24. Cleeren F, Lecina J, Bridoux J, et al. Direct fluorine-18 labeling of heat-sensitive biomolecules for positron emission tomography imaging using the Al^{18}F-RESCA method. *Nat Protoc.* 2018;13:2330–2347.
25. Wu Q, Wu Y, Zhang Y, et al. ImmunoPET/CT imaging of clear cell renal cell carcinoma with [^{18}F]RCCB6: a first-in-human study. *Eur J Nucl Med Mol Imaging.* 2024;51:2444–2457.
26. Qin X, Guo X, Liu T, et al. High in-vivo stability in preclinical and first-in-human experiments with [^{18}F]AlF-RESCA-MIRC213: a ^{18}F-labeled nanobody as PET radiotracer for diagnosis of HER2-positive cancers. *Eur J Nucl Med Mol Imaging.* 2023;50:302–313.
27. Liu J, Guo X, Wen L, et al. Comparison of renal clearance of [^{18}F]AlF-RESCA-HER2-BCH and [^{18}F]AlF-NOTA-HER2-BCH in mice and breast cancer patients. *Eur J Nucl Med Mol Imaging.* 2023;50:2775–2786.
28. Nelson BE, Meric-Bernstam F. Leveraging TROP2 antibody-drug conjugates in solid tumors. *Annu Rev Med.* 2024;75:31–48.
29. Wang J, Wu L, Song Z, et al. A first-in-human (FIH) phase 1 study of SHR-A1921, a TROP-2 targeted antibody-drug conjugate (ADC), in patients with advanced solid tumors [abstract]. *Cancer Res.* 2023;83(suppl):CT181.
30. Liu X, Ma L, Li J, et al. Trop2-targeted therapies in solid tumors: advances and future directions. *Theranostics.* 2024;14:3674–3692.
31. Herrmann K, Schwaiger M, Lewis JS, et al. Radiotheranostics: a roadmap for future development. *Lancet Oncol.* 2020;21:e146–e156.
32. Bodei L, Herrmann K, Schoder H, Scott AM, Lewis JS. Radiotheranostics in oncology: current challenges and emerging opportunities. *Nat Rev Clin Oncol.* 2022;19:534–550.
33. Wang C, Chen Y, Hou YN, et al. ImmunoPET imaging of multiple myeloma with [^{68}Ga]Ga-NOTA-Nb1053. *Eur J Nucl Med Mol Imaging.* 2021;48:2749–2760.
34. Larson SM, Carrasquillo JA, Cheung NK, Press OW. Radioimmunotherapy of human tumours. *Nat Rev Cancer.* 2015;15:347–360.
35. Shvartsur A, Bonavida B. Trop2 and its overexpression in cancers: regulation and clinical/therapeutic implications. *Genes Cancer.* 2015;6:84–105.
36. Stepan LP, Trueblood ES, Hale K, Babcook J, Borges L, Sutherland CL. Expression of Trop2 cell surface glycoprotein in normal and tumor tissues: potential implications as a cancer therapeutic target. *J Histochem Cytochem.* 2011;59:701–710.